MULTISTEP ELECTROCHEMICAL REDUCTION PATH OF CLUSTERS $[Os_3(CO)_{10}(\alpha\text{-DIIMINE})]$: COMPARISON OF ELECTROCHEMICAL AND PHOTOCHEMICAL Os–Os(α-DIIMINE) BOND CLEAVAGE

František HARTL[1,*] and Josephina W. M. van OUTERSTERP

Van't Hoff Institute for Molecular Sciences, University of Amsterdam, Nieuwe Achtergracht 166, 1018 WV Amsterdam, The Netherlands; e-mail: [1] hartl@science.uva.nl

Received January 3, 2006
Accepted February 15, 2006

Dedicated to Professor Jaroslav Podlaha on the occasion of his 70th birthday.

Electrochemical reduction of the triangular clusters $[Os_3(CO)_{10}(\alpha\text{-diimine})]$ (α-diimine = 2,2′-bipyridine (bpy), 2,2′-bipyrimidine (bpym)) and $[Os_3(CO)_{10}(\mu\text{-bpym})ReBr(CO)_3]$ produces primarily the corresponding radical anions. Their stability is strongly determined by the π-acceptor ability of the reducible α-diimine ligand, which decreases in the order μ-bpym > bpym >> bpy. Along this series, increasing delocalisation of the odd electron density in the radical anion over the Os(α-diimine) chelate ring causes weakening of the axial $(CO)_4Os–Os(CO)_2(\alpha\text{-diimine})$ bond and its facile cleavage for α-diimine = bpy. In contrast, the cluster radical anion is inherently stable for the bridging bpym ligand, the strongest π-acceptor in the studied series. In the absence of the partial delocalisation of the unpaired electron over the Re(bpym) chelate bond, the Os_3-core of the radical anion remains intact only at low temperatures. Subsequent one-electron reduction of $[Os_3(CO)_{10}(bpym)]^{\bullet-}$ at T = 223 K gives the open-triosmium core (= Os_3*) dianion, $[Os_3*(CO)_{10}(bpym)]^{2-}$. Its oxidation leads to the recovery of parent $[Os_3(CO)_{10}(bpym)]$. At room temperature, $[Os_3*(CO)_{10}(bpym)]^{2-}$ is formed along a two-electron (ECE) reduction path. The chemical step (C) results in the formation of an open-core radical anion that is directly reducible at the cathodic potential of the parent cluster in the second electrochemical (E) step. In weakly coordinating tetrahydrofuran, $[Os_3*(CO)_{10}(bpym)]^{2-}$ rapidly attacks yet non-reduced parent cluster molecules, producing the relatively stable open-core dimer $[Os_3*(CO)_{10}(bpym)]_2^{2-}$ featuring two open-triangle cluster moieties connected with an (bpym)Os–Os(bpym) bond. In butyronitrile, $[Os_3*(CO)_{10}(bpym)]^{2-}$ is stabilised by the solvent and the dimer $[Os_3*(CO)_{10}(bpym)]_2^{2-}$ is then mainly formed by reoxidation of the dianion on reverse potential scan. The more reactive cluster $[Os_3(CO)_{10}(bpy)]$ follows the same reduction path, as supported by spectroelectrochemical results and additional valuable evidence obtained from cyclic voltammetric scans. The ultimate process in the reduction mechanism is fragmentation of the cluster core triggered by the reduction of the dimer $[Os_3*(CO)_{10}(\alpha\text{-diimine})]_2^{2-}$. The products formed are $[Os_2(CO)_8]^{2-}$ and $\{Os(CO)_2(\alpha\text{-diimine})\}_2$. The latter dinuclear fragments constitute a linear polymeric chain $[Os(CO)_2(\alpha\text{-diimine})]_n$ that is further reducible at the α-diimine ligands. For α-diimine = bpy, the charged polymer is capable of reducing carbon dioxide. The electrochemical opening of the triosmium core in the $[Os_3(CO)_{10}(\alpha\text{-diimine})]$ clusters exhibits

Collect. Czech. Chem. Commun. 2006, Vol. 71, No. 2, pp. 237–263

doi:10.1135/cccc20060237

several common features with their photochemistry. The same Os–α-diimine bond dissociates in both cases but the intimate mechanisms are different.

Keywords: Osmium clusters; α-Diimine ligands; Electrochemical reduction; Spectroelectrochemistry; Cyclic voltammetry; Organometallic polymers; Zwitterions; IR spectroscopy; Photochemistry.

Current interest in electrochemical properties and photochemical activation of oligo- and polynuclear low-valent ruthenium carbonyls with donor α-diimine ligands has been evoked between the mid-1980s and mid-1990s by a series of reports on a remarkably high heterogeneous catalytic activity and selectivity of the supported $[Ru_3(CO)_{12}]$/2,2′-bipyridine system in the water–gas shift reaction (WGSR) as well as hydroformylation and isomerisation of olefins[1]. The nature of the pre-catalyst surface species was resolved in 1996 by diffuse reflectance FTIR spectroscopic studies of $[Ru_3(CO)_{12}]$/2,2′-bipyridine/SiO_2 samples (prepared by impregnation from non-chlorinated solvents or by a gas-phase method). Thermal treatment of the physisorbed triangular cluster with 2,2′-bipyridine (bpy) was shown to produce air-sensitive linear chains $[Ru(CO)_2(bpy)]_n/SiO_2$ as the dominant surface species[2]. Poorly soluble $[Ru(CO)_2(bpy)]_n$ was also prepared independently by electrochemical two-electron reduction of *trans*(Cl)-$[RuCl_2(CO)_2(bpy)]$ and related mononuclear complexes. The reduction path involves intermediate formation of dimeric and tetrameric species with formally Ru^I-bpy terminal units concomitantly reducible at the applied cathodic potential of the parent complex[3]. The polymeric ruthenium product (the average chain length, estimated by X-ray powder diffraction, is ca. 60 Å, with Ru–Ru distances close to 3 Å)[4] is also highly active in electrocatalytic reduction of CO_2 to CO and formate[3b,5]. A similar reactivity towards CO_2 was recently reported for $[Os(CO)_2(bpy)]_n$ prepared by electrochemical reduction of *trans*(Cl)-$[OsCl_2(CO)_2(bpy)]$ (ref.[6]). Notably, the Os(II) and reduced Os(0) complexes proved to be better suited for mechanistic spectro-electrochemical studies than the more reactive ruthenium derivatives[7].

The catalytic activity of the $[Ru_3(CO)_{12}]$/2,2′-bipyridine system suggests that the actual catalyst, $[Ru(CO)_2(bpy)]_n$, is also formed in the course of electrochemical reduction of the substituted cluster $[Ru_3(CO)_8(\mu\text{-}CO)_2(bpy)]$ containing two carbonyl ligands bridging over one of the Ru–Ru bonds[8]. This presumption was recently confirmed for 2,2′-bipyridine and also for the stronger π-acceptor 2,2′-bipyrimidine[9]. Remarkably, closely related

polymer $[Ru(CO)_2(i\text{Pr-AcPy})]_n$ (*i*Pr-AcPy = 2-acetylpyridine *N*-isopropylimine; see Chart 1) was also generated by exhaustive reduction of the heterometallic cluster $[RuOs_2(CO)_{10}(i\text{Pr-AcPy})]$, with the α-diimine ligand chelating the Ru centre. In the latter case, the formation of $[Ru(CO)_2(i\text{Pr-AcPy})]_n$ together with $[Os_2(CO)_8]^{2-}$ pointed to the existence of an intermediate dimeric cluster featuring a (*i*Pr-AcPy)Ru–Ru(*i*Pr-AcPy) bond that remained preserved in the subsequent cathodic polymerisation process. In this regard, it is important to note that the description of the reduction paths of both $[Ru_3(CO)_8(\mu\text{-}CO)_2(bpy)]$ and $[RuOs_2(CO)_{10}(i\text{Pr-AcPy})]$ has been mainly based on largely unpublished spectroscopic evidence obtained earlier with $[Os_3(CO)_{10}(bpy)]$ and related triosmium clusters[10]. To date, only preliminary data have been reported for $[Os_3(CO)_{10}(i\text{Pr-PyCa})]$ (*i*Pr-PyCa = σ-*N*,σ-*N*′-bound pyridine-2-carbaldehyde *N*-isopropylimine; see Chart 1) in a spectroelectrochemical and quantum-chemical study that was mainly devoted to derivatives with ortho-metallated α-diimine ligands[11]. The thorough description of the intriguing reduction pathway of $[Os_3(CO)_{10}(\alpha\text{-diimine})]$ is presented for the first time in this article for chelating α-diimine = 2,2′-bipyridine (cluster **3**) and 2,2′-bipyrimidine, bpym (non-bridging in cluster **2** and forming a bridge between the cluster core and the $ReBr(CO)_3$ moiety in compound **1**), see Chart 1. The reactivity induced by the electrochemical reduction of these clusters is compared with their interesting photochemistry[12] involving solvent-, temperature- and α-diimine-dependent formation of open-core biradical and zwitterionic triosmium species. These photoproducts are closely related to some of the species formed along the reduction path.

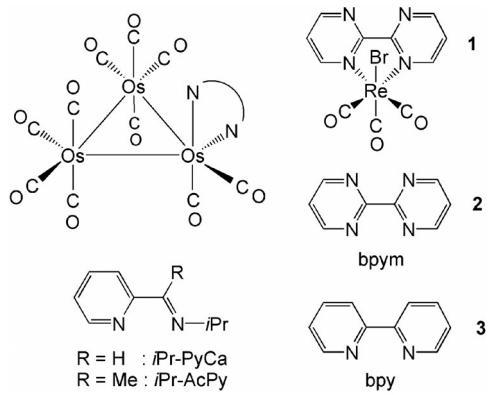

CHART 1

EXPERIMENTAL

General Remarks

All reactions and experiments were performed under an inert atmosphere of dry nitrogen, using standard Schlenk techniques. Acetonitrile solutions of photoreactive clusters were handled under exclusion of daylight.

All solvents used (Acros) were of analytical grade. Dry tetrahydrofuran (THF) and hexane were obtained by distillation from Na/benzophenone and butyronitrile (PrCN) from P_2O_5. 1,2-Dimethoxyethane (DME) was pre-dried with $CaCl_2$ and refluxed with CaH_2. The supporting electrolyte, tetrabutylammonium hexafluorophosphate (TBAH; Aldrich), was recrystallised twice from absolute ethanol and dried overnight at 80 °C under vacuum before use. Silica 60 (70–230 mesh, Merck) for column chromatography were activated by heating overnight at 180 °C under vacuum and stored under N_2. Ferrocene (BDH), and cobaltocene (Aldrich) were used as received. $[Fe(\eta^5\text{-}C_5H_5)(\eta^6\text{-}C_6Me_6)][PF_6]$ was synthesised according to a literature procedure[13] and reduced to the neutral 19-electron species $[Fe(\eta^5\text{-}C_5H_5)(\eta^6\text{-}C_6Me_6)]$ with 1% Na/Hg in dry DME [14]. The elemental analysis was carried out by Dornis und Kolbe, Mikroanalytisches laboratorium, Mülheim a.d. Ruhr, Germany.

Clusters $[Os_3(CO)_{10}(bpym)]$ (**2**)[12d] and $[Os_3(CO)_{10}(bpy)]$ (**3**)[12d,15] were prepared as described elsewhere. Their identity and purity was checked by recording their IR, ^{1}H NMR and FD^+ mass spectra.

The cluster $[Os_3(CO)_{10}(\mu\text{-bpym})ReBr(CO)_3]$ (**1**) was synthesised straightforwardly by stirring equimolar amounts of $[Os_3(CO)_{10}(bpym)]$ and $[ReBr(MeCN)_2(CO)_3]$ (ref.[16]) in THF under a nitrogen atmosphere overnight. The dark red solid obtained by solvent evaporation was purified by column chromatography over silica with gradient elution with THF/hexane. The dark red fractions were evaporated to dryness. For $C_{21}H_6BrN_4O_{10}OsRe$ (1275.0) calculated: 16.96% C, 0.47% H, 4.39% N; found: 17.08% C, 0.36% H, 4.47% N. ^{1}H NMR (300.13 MHz, acetone-d_6, 293 K): 10.05 (2 H, d); 9.65 (2 H, d); 8.13 (2 H, dd).

Spectroscopic Measurements

^{1}H NMR measurements (δ, ppm) were carried out on a Bruker AMX 300 spectrometer. X-band EPR spectra were recorded with a computer-controlled Varian Century E-104A spectrometer and simulated with the programs PEST WinSIM [17] and Bruker WINEPR SimFonia (version 1.25). The *g*-values were determined against 2,2-diphenyl-1-picrylhydrazyl (DPPH; Aldrich) used as an external standard (g = 2.0037)[18]. Infrared spectra were obtained with a Bio-Rad FTS-7 FTIR spectrometer (16 scans, resolution of 2 cm^{-1}). Electronic absorption spectra were recorded using a Hewlett–Packard 8453A diode-array and software-updated P-E Lambda 5 spectrophotometers.

Cyclic Voltammetry and Spectroelectrochemistry

Conventional cyclic voltammograms were recorded with a PAR EG&G Model 283 potentiostat, using an airtight, light-protected, single-compartment cell placed in a Faraday cage. The working electrode was a Pt microdisk polished with a 0.25 μm diamond paste between the scans. Coiled Pt and Ag wires served as an auxiliary and pseudoreference electrode, respectively. The sample concentration was typically 10^{-3} mol dm^{-3}. Ferrocene (Fc) was used as the internal standard[19] for the determination of electrode potentials and comparison of peak-

to-peak potential differences. Conversion of the Fc/Fc^+ potential scale to other reference systems can be found elsewhere[20]. The apparent number of electrons consumed by the studied clusters during irreversible reduction on the time scale of conventional cyclic voltammetry was determined according to a published procedure[21], using combination of diffusion-controlled and steady-state techniques, viz. chronoamperometry at the Pt disk microelectrode and slow-scan cyclic voltammetry at a home-made 10-μm Pt disk ultramicroelectrode, respectively. The diffusion coefficients were first estimated from reversible cyclic voltammetric responses, using ferrocene as internal standard.

IR and UV-VIS spectroelectrochemical experiments at room temperature were performed with an optically transparent thin-layer electrochemical (OTTLE) cell equipped with CaF_2 windows and a Pt minigrid working electrode (32 wires per cm)[22]. IR spectroelectrochemistry at low temperatures was conducted with a home-made cryostatted OTTLE cell[23]. The solutions were typically 3×10^{-3} mol dm^{-3} in the supporting electrolyte and 10^{-3} mol dm^{-3} (UV-VIS) or 5×10^{-3} mol dm^{-3} (IR) in the analyte. Working-electrode potential of the spectroelectrochemical cells was controlled with a PA4 potentiostat (Ekom, Polná, Czech Republic). A thin-layer cyclic voltammogram was recorded in the course of each spectroelectrochemical experiment to localize the redox events. Rapid electrolysis (within seconds at room temperature) at preselected potentials was achieved by the potential-step method.

Chemical reductions were performed with cobaltocene ($E_{1/2}$ = –1.33 V vs Fc/Fc^+) and $[Fe^I(\eta^5\text{-}C_5H_5)(\eta^6\text{-}C_6Me_6)]$ ($E_{1/2}$ = –1.99 V vs Fc/Fc^+).

RESULTS AND DISCUSSION

Electrochemical reduction potentials and IR ν(CO) wavenumbers of the triosmium clusters under investigation are presented in Tables I and II, respectively. Molecular structures of the various redox intermediates and products are visualised in Chart 2 for better orientation; the general symbol **X** stands for the cluster numbers **1**–**3** defined in Chart 1. The individual redox steps are thoroughly discussed in the following sections.

*Reduction Path of $[Os_3(CO)_{10}(\mu\text{-}bpym)ReBr(CO)_3]$ (**1**)*

One-electron reduction of cluster **1** to $\mathbf{1}^{\bullet-}$ in butyronitrile at $E_{1/2}$ = –0.93 V vs Fc/Fc^+ is fully reversible at room temperature at cyclic voltammetric scan rates v = 20 mV s^{-1} or higher. The fairly low cathodic potential is in line with the strong π-acceptor properties of the bridging bpym ligand[24]. The following cathodic wave in the cyclic voltammogram of **1** at $E_{p,c}$ = –1.56 V (v = 100 mV s^{-1}) is broader and totally irreversible, pointing to rapid decomposition of $\mathbf{1}^{2-}$.

The low reduction potential of cluster **1** nicely corresponds with its low-energy absorption in the visible region of the electronic absorption spectrum. The absorption bands of cluster **1** at 694 and 498 nm (in THF) probably belong to metal-to-ligand charge-transfer (MLCT) electronic transitions

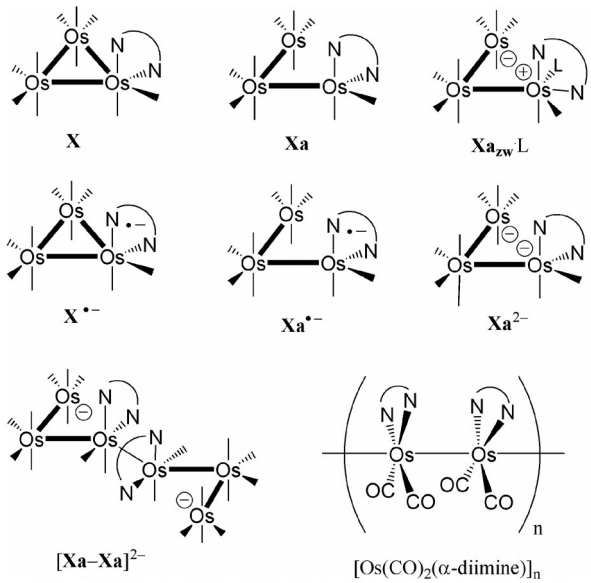

CHART 2

TABLE I
Electrochemical reduction potentials of the studied triosmium clusters (Chart 1), their radical anions and open-core zwitterions[a]

Compound	$E_{1/2}$[b], V			
Parent cluster (α-diamine)	**1** (μ-bpym)	**2** (bpym)	(*i*Pr-PyCa)[c]	**3** (bpy)
	–0.93	–1.51	*–1.77*	*–1.85*
		–1.47[d]	–1.73[e]	–1.84[e]
Radical anion	**1**$^{\bullet-}$	**2**$^{\bullet-}$		**3**$^{\bullet-}$
	–1.56	*–1.96*	*–2.23*[e]	[f]
				–2.24[e]
Zwitterion				**3a**$_{zw}$·L
L = CO			*–1.56*[g]	*–1.75*[g]
L = pyridine				*–1.80*[h]

[a] Experimental conditions: Cyclic voltammetry (electrode potentials vs Fc/Fc$^+$), 10^{-1} M TBAH in THF, T = 293 K, v = 100 mV s^{-1} (unless stated otherwise); Pt microelectrode. [b] $E_{p,c}$ values for completely irreversible cathodic steps given in italics. [c] [Os$_3$(CO)$_{10}$(*i*Pr-PyCa)], ref.[11]. [d] In PrCN. [e] T = 200 K. [f] Not observed. [g] In CO-saturated THF. [h] In THF/pyridine 4:1; formed by oxidation of open-core cluster dianion **3a**$^{2-}$.

TABLE II
Infrared CO-stretching frequencies of the studied clusters $[Os_3(CO)_{10}(\mu\text{-bpym})ReBr(CO)_3]$ (**1**) and $[Os_3(CO)_{10}(\alpha\text{-diimine})]$ (α-diimine = bpym (**2**), bpy (**3**)), and products resulting from their reduction (Chart 2)

Compound	ν(CO), cm^{-1}
1[a,b]	2092m, 2044m-s, 2028vs, 2013s-m, 2001s, 1990sh, 1971sh, 1933m, 1912m
1[b,c]	2092m, 2045m, 2029vs, 2012sh, 2004s, 1988sh, 1965sh, 1932m, 1916m
$\mathbf{1}^{\bullet-}$ [b,c]	2079w, 2068vw, 2026s-m, 2014vs, 1992s,br, 1971sh, 1948w, 1909m, 1892m
$\mathbf{1}^{\bullet-}$ [a,b]	2078w, 2042sh, 2021s, 2014vs, 1999m-s, 1990sh, 1970sh, 1901s,br
$\mathbf{1}^{\bullet-}$ [a,b,d]	2079w, 2063w, 2042w, 2022sh, 2013vs, 1996s, 1988s, 1970sh, 1949sh, 1906s, 1890s
P1a[b,c]	2053w, 2022s, 2004m, 1966vs,br, 1921m-s, 1902m-s, 1883m-s, 1865sh
2[a,b]	2086m, 2035vs, 2004vs, 1992vs, 1979s, 1957m, 1907w-m
2[c,e]	2086m, 2035s, 2003sh, 1995vs, 1977s, 1958m, 1902w-m
$\mathbf{2}^{\bullet-}$ [a,b]	2072w, 2062w, 2016s, 1986sh, 1981vs, 1963s, 1941m, 1901w
$\mathbf{2}^{\bullet-}$ [c,e]	2075vw, 2063w, 2017s-m, 1989sh, 1979vs, 1966s, 1944m, 1881w
$[\mathbf{2a}–\mathbf{2a}]^{2-}$ [a,b]	2061w, 1980vs, 1966s, 1892w, 1872w-m
$[\mathbf{2a}–\mathbf{2a}]^{2-}$ [b,c,f]	2060vw, 1977vs, 1967sh, 1899w, 1868w
P2a[a,b]	2058w,br, 1966vs, 1888m-w, 1865m
$[\mathbf{2a}]^{2-}$ [b,c]	2053vw, 2018vw, 1962vs, 1942s, 1886w, 1853w-m
$[\mathbf{2a}]^{2-}$ [c,e]	2056vw, 2014vw, 1960vs, 1941s-m, 1883w, 1850w-m
3[a,b]	2083m, 2031s, 2000s, 1990vs, 1973s, 1952m, 1901w-m
3[b,c]	2084m, 2032s, 1994vs,br, 1976s, 1952sh, 1899w-m
3[c,e]	2083m, 2032s, 1995vs,br, 1974s, 1954sh, 1896w
$[\mathbf{3a}–\mathbf{3a}]^{2-}$ [a,b]	2056w, 1972vs, 1946sh, 1881sh, 1861m-w
$[\mathbf{3a}–\mathbf{3a}]^{2-}$ [a,b,g]	2055w, 1969vs, 1945s-m, 1881sh, 1864m-w
$[\mathbf{3a}–\mathbf{3a}]^{2-}$ [b,c]	2054w, 1970vs,br, 1945sh, 1881sh, 1864m-w
$[\mathbf{3a}–\mathbf{3a}]^{2-}$ [c,h]	2054w, 1966vs,br, 1945sh, 1880sh, 1861m-w
$\mathbf{3a}^{2-}$ [c,i,j]	2050vw, 1957vs, 1944sh, 1852m,br

[a] In THF. [b] T = 293 K. [c] In PrCN. [d] Reduction of **1** with 1 equiv. cobaltocene. [e] T = 223 K. [f] Oxidation of $\mathbf{2a}^{2-}$. [g] Reduction of **3** with 1 equiv. $[Fe(\eta^5\text{-}C_5H_5)(\eta^6\text{-}C_6Me_6)]$. [h] At T = 253 K. [i] At T = 200 K. [j] In mixture with $[\mathbf{3a}–\mathbf{3a}]^{2-}$ (identical wavenumbers at T = 253 and 200 K); the wavenumbers of $\mathbf{3a}^{2-}$ correspond to the absorbance difference spectrum.

originating from the Os and Re metal centres, respectively, both being directed to the low-lying unoccupied π* level(s)[25] of the bridging bpym ligand. In the spectrum of one-electron-reduced $\mathbf{1}^{\bullet-}$, formed in situ within the spectroelectrochemical cell (see Experimental), two new, yet unassigned absorption bands arise at 585 and 443 nm. It is noteworthy that similar spectral changes have been reported for the related complex $[(CO)_5Mn–Re^0(CO)_3(\mu\text{-bpym})Re^IBr(CO)_3]$, showing two Re-to-bpym charge-transfer bands at λ_{max} = 473 nm (Re^I) and 671 nm (Re^0), and its radical anion with two broad visible absorption bands of lower intensity, positioned at higher energy[24b]. A detailed study of the electronic transitions in the radical anions was beyond the scope of this work.

The IR ν(CO) pattern of cluster **1** remained preserved in $\mathbf{1}^{\bullet-}$ but shifted to smaller wavenumbers by ca. 20 cm^{-1} (Table II, Fig. 1). This shift reflects an increased π-back-donation from Re and Os to the carbonyl ligands, caused by the added single electron mainly localised on the bridging bpym ligand[24].

Radical anion $\mathbf{1}^{\bullet-}$ is inherently stable at room temperature, independently of the solvent used (THF or PrCN). It could also be obtained smoothly by chemical reduction with cobaltocene in THF at 293 K (Table II). The EPR signal of the air-sensitive product was observed at g = 1.9939 as a poorly resolved sextet (Fig. 2). The hyperfine structure originates from the interaction of the unpaired electron with the ^{185,187}Re nuclei (I = 5/2). It was fully reproduced by spectral simulation that gave a(Re) = 1.22 mT. This value and the field position of the EPR signal are close to the parameters determined for the stable radical anion $[ReCl(CO)_3(bpym)]^{\bullet-}$ (g = 2.0086, a(Re) = 1.0 mT)[26] and dinuclear $[\{ReBr(CO)_3\}_2(\mu\text{-bpym})]^{\bullet-}$ (g = 2.0005, a(Re) =

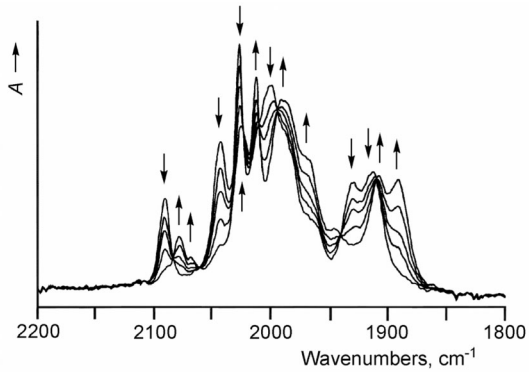

FIG. 1
One-electron reduction of cluster **1** to $\mathbf{1}^{\bullet-}$ monitored by IR spectroscopy. Conditions: THF, T = 293 K, electrolysis in an OTTLE cell

1.2 mT)[27]. The apparent delocalisation of the odd electron density over the Re(bpym) chelate ring in $\mathbf{1}^{\bullet-}$ increases significantly the stability of the triosmium core, as will be documented below for cluster **2** with the non-bridging bpym ligand.

The subsequent irreversible reduction of radical anion $\mathbf{1}^{\bullet-}$ at $E_{p,c}$ = –1.56 V, in PrCN at 293 K, was monitored with IR spectroscopy. The product **P1a** shows a considerably different ν(CO) pattern compared to that of the parent compound, which excludes its assignment as $\mathbf{1}^{2-}$: 2053w, 2022s, 2004m, 1966vs,br, 1921m-s, 1902m-s and 1883m-s, 1865sh cm^{-1}. The exact molecular structure of **P1a** has not been elucidated so far. Nevertheless, the IR ν(CO) bands with the underlined wavenumbers indicate that the second cathodic step causes opening of the triosmium core, as described in detail below for cluster **2**: cf. the IR spectrum of the open-core species, **P2a**, in Table II.

Finally, electrochemical reduction of **P1** at more negative potentials results in cluster fragmentation (also observed for **P2a**, see below), as revealed by new ν(CO) bands at 1936s-m and 1864vs cm^{-1} attributed to $[Os_2(CO)_8]^{2-}$ (ref.[28]). Another product of this cathodic process, showing ν(CO) bands at 2007s and 1885s,br cm^{-1}, can be assigned as the solvent-substituted radical $[Re(CO)_3(bpym)(PrCN)]^{\bullet}$, with the low-frequency "E" band unresolved due to the C_{3v} spectroscopic symmetry of the ReC_3N_3 core[26]. For comparison, the radical anion $[ReBr(CO)_3(bpym)]^{\bullet-}$ absorbs in PrCN at 2004, 1897 and 1877 cm^{-1}, and $[Re(CO)_3(bpym)(THF)]^{\bullet}$ in THF at 2012, 1914 and 1893 cm^{-1} (ref.[24b]). It cannot be excluded that the Br^- ligand at the Re centre is substituted by PrCN already during the preceding reduction of $\mathbf{1}^{\bullet-}$ and formation

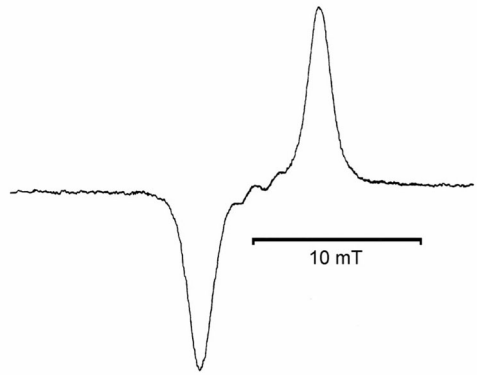

FIG. 2
EPR spectrum of radical anion $\mathbf{1}^{\bullet-}$ recorded after reduction of parent cluster **1** with cobaltocene in THF at T = 293 K

of product **P1a**. Another open point is whether the $Os(CO)_2$ moiety remains chelated by the bpym ligand after the reduction-induced fragmentation of the cluster core; this holds well for clusters **2** and **3**, see below.

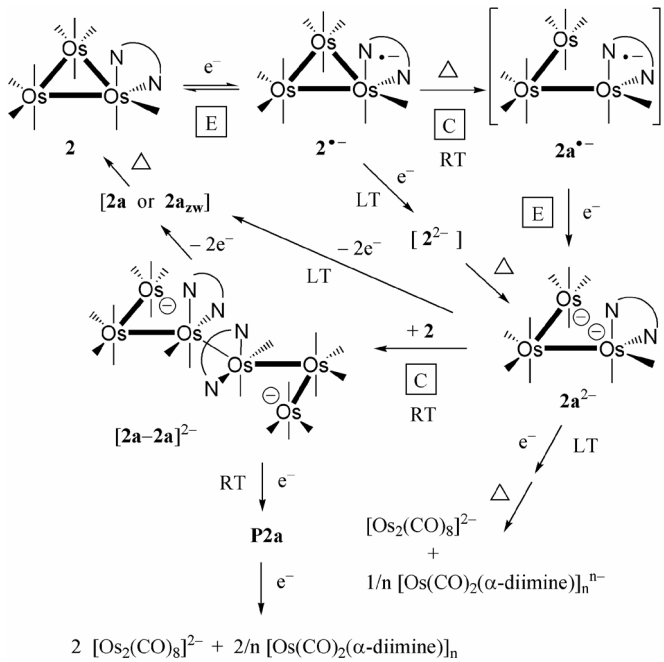

SCHEME 1

Electrochemical reduction and reoxidation paths of $[Os_3(CO)_{10}(bpym)]$ (**2**) constructed on the basis of the available experimental data, see below. The symbols E and C denote the (one-electron) electrochemical and chemical steps, respectively, in the reaction mechanism. The symbol Δ stands for a thermal reaction

*Reduction Path of $[Os_3(CO)_{10}(bpym)]$ (**2**)*

Similar to cluster **1**, the cyclic voltammogram of cluster **2** shows a cathodic wave at $E_{1/2}$ = –1.51 V (THF) or –1.47 V (PrCN), which is fully reversible at room temperature in both solvents. The reduction potential is more negative by ca. –0.6 V than that of cluster **1**, which reflects a higher LUMO energy and significantly decreased acceptor capacity of the non-bridging bpym ligand in cluster **2**. The reduction of **2** is diffusion controlled, as confirmed by usual diagnostic tests[29]. The diffusion coefficient of cluster **2** has been determined: $D_2 = (0.22 \pm 0.03)/D_{Fc}$ (ferrocene was used as internal standard; $D_{Fc} = 8.0 \times 10^{-6}$ cm^2 s^{-1} in THF [24a]). Whereas one-electron-reduced

$\mathbf{2}^{\bullet-}$ remains stable on the time scale of cyclic voltammetry, $\mathbf{2}^{2-}$ formed in the following cathodic step (Table II) rapidly decomposes and the anodic counter-peak is absent at $v \leq 50$ V s^{-1}.

IR spectroelectrochemical investigation of the reduction of cluster **2** started in PrCN at 223 K. Radical anion $\mathbf{2}^{\bullet-}$ was found fully stable under these circumstances. The assignment was again aided by the retention of the ν(CO) pattern of **2** shifted due to the additional electron in $\mathbf{2}^{\bullet-}$ to lower frequencies (Table II, Fig. 3). The UV-VIS spectrum of $\mathbf{2}^{\bullet-}$ shows a characteristic feature of a reduced species with the odd electron localised on the chelating bpym ligand[30], viz. two sharp absorption maxima at 464 and 490 nm.

In contrast to stable $\mathbf{1}^{\bullet-}$, the lifetime of $\mathbf{2}^{\bullet-}$ at room temperature is short. In THF, $\mathbf{2}^{\bullet-}$ could be observed by IR spectroscopy at fairly high concentration only when performing the reduction of **2** in a potential-step fashion, on the time scale of seconds. During a slow potential scan (v = 2 mV s^{-1}), the detectable amount of $\mathbf{2}^{\bullet-}$ formed was very small. The reactivity increases in PrCN, where no $\mathbf{2}^{\bullet-}$ could be observed during the spectroelectrochemical experiment at room temperature independently of the electrolysis rate.

The thermal reaction of $\mathbf{2}^{\bullet-}$ in THF at room temperature yields a stable species showing an IR ν(CO) pattern characteristic of the triosmium core with one of the Os–Os(α-diimine) bonds broken, $[Os_3{}^*(CO)_{10}(bpym)]$ (**2a**) (Fig. 4). These structures are known to be generated photochemically (for bpym, bpy and other α-diimine ligands), for example as biradicals $[Os^{\bullet}(CO)_4–Os(CO)_4–Os^{+}(L)(CO)_2(\alpha\text{-diimine}^{\bullet-})]$ (L = Lewis base; **2a**·L) or zwit-

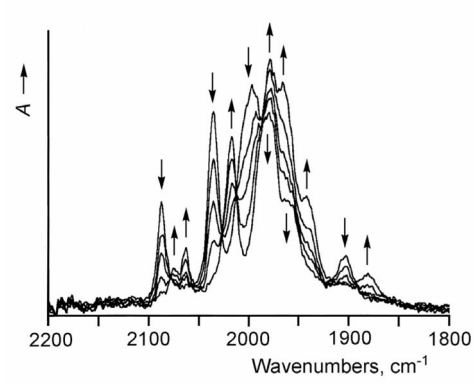

FIG. 3
One-electron reduction of cluster **2** to $\mathbf{2}^{\bullet-}$ monitored by IR spectroscopy. Conditions: PrCN, T = 223 K, electrolysis in an OTTLE cell

terions $[Os^{-}(CO)_4–Os(CO)_4–Os^{+}(L)(CO)_2(\alpha\text{-diimine})]$ ($\mathbf{2a_{zw}}\cdot L$) by splitting of an Os–Os(α-diimine) bond from a core-to-α-diimine ($\sigma\pi^*$) excited state of $[Os_3(CO)_{10}(\alpha\text{-diimine})]$ (ref.[12]). Importantly, as shown in Fig. 5, a remarkable coincidence exists between the ν(CO) pattern and wavenumbers of the secondary reduction product formed out of $\mathbf{2}^{\bullet-}$ at 293 K and the zwitterion stabilised by coordination of the Br^- ligand to the $Os^{+}(CO)_2$(bpym) site, $\mathbf{2a_{zw}}\cdot Br^-$ (i.e., an anionic open-core species)[12d]. The EPR-silent electrochemical product has been assigned as $[\mathbf{2a}–\mathbf{2a}]^{2-}$, i.e., as a cluster dimer with two open-core $\{Os_3^*(CO)_{10}(bpym)\}$ moieties linked with a (bpym)Os–Os(bpym) bond, each bearing a terminal $Os^{-}(CO)_4$ group (Scheme 1). As already

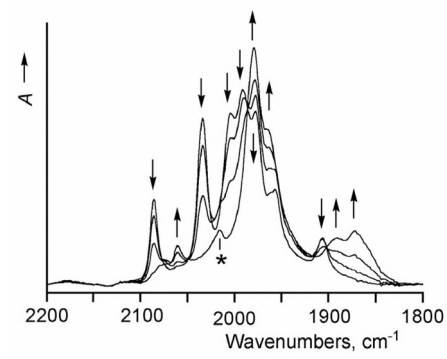

FIG. 4
Overall one-electron reduction of cluster **2** to $[\mathbf{2a}–\mathbf{2a}]^{2-}$ (Scheme 1) monitored by IR spectroscopy. Conditions: THF, T = 293 K, electrolysis in an OTTLE cell. The asterisk denotes a small amount of $\mathbf{2}^{\bullet-}$

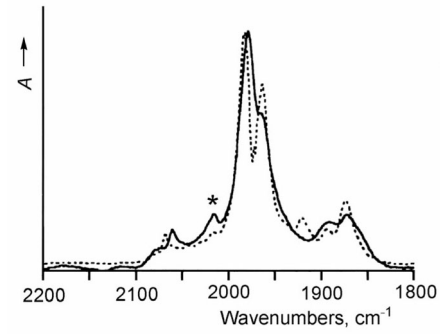

FIG. 5
Comparison of IR spectra of cluster dimer $[\mathbf{2a}–\mathbf{2a}]^{2-}$ (full line) and isoelectronic open-core photoproduct $[Os^{-}(CO)_4–Os(CO)_4–Os^{+}(Br)(CO)_2(\alpha\text{-diimine})]^{-}$ (dotted line). Both spectra were recorded in THF at 293 K. The asterisk denotes a small amount of $\mathbf{2}^{\bullet-}$

pointed out above, the most conclusive evidence for the unusual dimeric cluster structure was obtained recently[31] from the electrochemical reduction of the heterometallic cluster $[Os_2(CO)_8Ru(CO)_2(i\text{Pr-AcPy})]$, where the corresponding (*i*Pr-AcPy)Ru–Ru(*i*Pr-AcPy) bonded dimer is the precursor of the linear polymer $[Ru(CO)_2(i\text{Pr-AcPy})]_n$ and the homodinuclear complex $[Os_2(CO)_8]^{2-}$.

Another important result was obtained by in situ electrochemical reduction of the primary radical anion, $\mathbf{2}^{\bullet-}$, in PrCN at 223 K. The product shows a very similar IR ν(CO) pattern as $[\mathbf{2a}–\mathbf{2a}]^{2-}$ but shifted to smaller wavenumbers by a magnitude corresponding to additional electron at the triosmium core (Fig. 6, Table II). We have, therefore, attributed the resulting IR spectrum to $\mathbf{2a}^{2-}$, i.e., an open-core triosmium cluster bearing negative charges at both terminal metal centres (Scheme 1).

When cluster **2** is reduced in PrCN at 293 K, slow voltammetric scan (v = 2 mV s^{-1}) using the OTTLE cell results in IR spectral changes that are identical to those observed in THF under these conditions, i.e., corresponding to the formation of dimer $[\mathbf{2a}–\mathbf{2a}]^{2-}$ (Table II). However, differently from the result in THF, much faster potential-step reduction of **2** in PrCN at –1.50 V (the faradaic current decayed to zero in a few seconds) yielded mainly open-core dianion $\mathbf{2a}^{2-}$ (Table II), together with a minor amount of dimer $[\mathbf{2a}–\mathbf{2a}]^{2-}$. Reverse oxidation of $\mathbf{2a}^{2-}$ at an electrode potential ca. 100 mV less negative than that of parent cluster **2** then generated exclusively $[\mathbf{2a}–\mathbf{2a}]^{2-}$ (Table II). In this regard it is important to note that reoxidation of

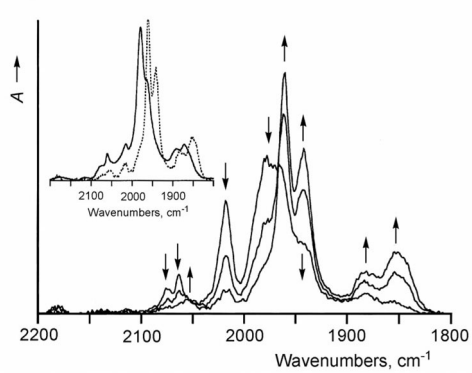

FIG. 6
One-electron reduction of cluster $\mathbf{2}^{\bullet-}$ to open-core $\mathbf{2a}^{2-}$ monitored by IR spectroscopy. Conditions: PrCN, T = 223 K, electrolysis in an OTTLE cell. Inset: comparison of IR spectra of dianion $\mathbf{2a}^{2-}$ (dotted line) and dimer $[\mathbf{2a}–\mathbf{2a}]^{2-}$ (full line; see Figs 4 and 5)

2a^{2-} at 223 K led directly to complete recovery of parent cluster **2**. The most plausible explanation of these results is that dianion **2a**$^{2-}$ is formed in the course of the reduction of **2** already prior to dimer [**2a**–**2a**]$^{2-}$ (Scheme 1). In analogy with the charge-transfer photoreactivity of **2** and related clusters[12], we may reasonably expect that radical anion **2**$^{\bullet-}$ transforms at elevated temperature by cleavage of an Os–Os(bpym) bond to its open-core equivalent **2a**$^{\bullet-}$ that is then directly reducible at the applied cathodic potential of parent cluster **2** to dianion **2a**$^{2-}$. This ECE process (Scheme 1) is not exceptional for mononuclear transition metal carbonyls. For example, it was reported to occur along the reduction paths of [$Fe(CO)_5$], [$Cr(CO)_6$] (ref.[32]) or [$MnBr(CO)_3$(bpy)] (ref.[21b]). The {$Os(CO)_2$(bpym)} moiety in **2** also belongs to this family. Dimer [**2a**–**2a**]$^{2-}$ is then the product of an efficient zero-electron reaction between strongly nucleophilic dianion **2a**$^{2-}$ and yet non-reduced **2**. This second chemical step in the ECEC sequence (Scheme 1) can be largely suppressed either at sufficiently low temperatures (creating a higher reaction barrier for the coupling) or by fast exhaustive electrolysis of **2** at room temperature. Apparently, an important role is also played by PrCN as a better donor solvent than THF. Weak coordination of PrCN at the $Os(CO)_2$(bpym) centre probably facilitates the cleavage of the Os–Os(bpym) bond in **2**$^{\bullet-}$ and, at the same time, protects dianion **2a**$^{2-}$ from the attack of **2**.

Further electrochemical reduction of dimer [**2a**–**2a**]$^{2-}$ at more negative potentials, in THF at 293 K, did not produce dianion **2a**$^{2-}$. Instead, it induced smooth formation of a new species denoted **P2a** (Table II), which exhibits IR and UV-VIS spectra similar to those of the precursor dimer (Figs 7 and 8). The UV-VIS spectra were recorded upon careful IR spectroscopic monitoring in the course of a combined spectroelectrochemical experiment. We do not like to speculate extensively about the molecular structure of **P2a** but some remarks can be made. The IR ν(CO) pattern reveals the presence of the open-core **2a** motif. However, it is unclear whether the (bpym)Os–Os(bpym) bond persisted in **P2a**. The ν(CO) wavenumbers lie between those of starting dimer [**2a**–**2a**]$^{2-}$ and two-electron-reduced **2a**$^{2-}$ (Table II). Differently from **2a**$^{2-}$, reoxidation of **P2a** did not produce [**2a**–**2a**]$^{2-}$ or starting cluster **2**, which indicates some irreversible structural change. Nevertheless, we consider **P2a** as a two-electron-reduced species, which agrees with its close relation to **P1a** generated by electrochemical reduction of radical anion **1**$^{\bullet-}$ (see above). In addition, further electrochemical reduction of both **P1a** and **P2a** induces fragmentation of the triosmium core, which was also observed for **2a**$^{2-}$ (see below).

The appearance of IR ν(CO) bands at 1935 and 1864 cm^{-1} due to $[Os_2(CO)_8]^{2-}$ in the course of the reduction of **P2a** indeed reveals the ultimate fragmentation of the triosmium cluster core. The other product of this process is probably the polymer $[Os(CO)_2(bpym)]_n$ absorbing at 1964 and ca. 1890 cm^{-1}. These wavenumbers are close to the literature values reported for $[Ru(CO)_2(bpym)]_n$ (ref.[9]) and $[Os(CO)_2(bpy)]_n$ (ref.[7]).

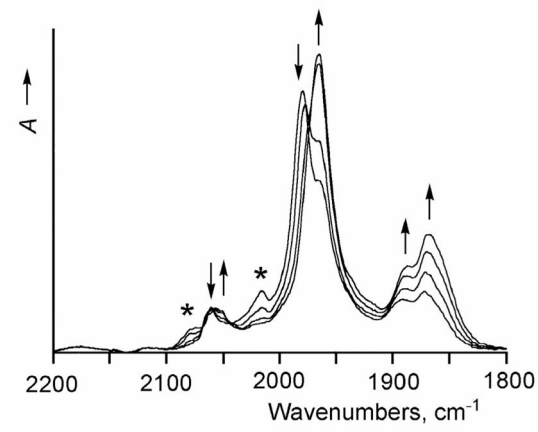

FIG. 7
Electrochemical conversion of dimer [**2a**–**2a**]$^{2-}$ to **P2a** monitored by IR spectroscopy. Conditions: THF, T = 293 K, electrolysis in an OTTLE cell. The asterisks denote a small amount of **2**$^{\bullet-}$

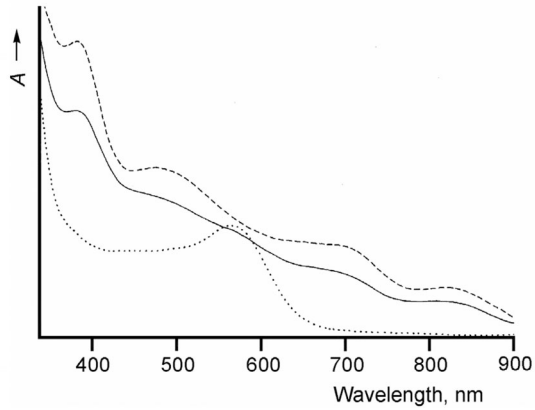

FIG. 8
UV-VIS spectra of parent cluster **2** (dotted line), dimer [**2a**–**2a**]$^{2-}$ (full line) and **P2a** (dashed line), recoded in THF at T = 293 K in an OTTLE cell

The cluster fragmentation and formation of $[Os_2(CO)_8]^{2-}$ was also observed during the reduction of dianion **2a**$^{2-}$ in PrCN at 223 K. In this case, the high-frequency ν(CO) band of the diosmium species lies at 1939 cm^{-1} and has a higher intensity than the 1964 cm^{-1} band, compared with the experiment in THF at 223 K. This difference points to an underlying ν(CO) band due to the reduced form of the linear polymer, $[Os(CO)_2(bpym)]_n^{n-}$ (ref.[7]), consistent with a more negative electrode potential of the **2a**$^{2-}$ reduction.

*Reduction Path of $[Os_3(CO)_{10}(bpy)]$ (**3**)*

It will be shown that the reduction path of cluster **3** (Scheme 2) does not deviate substantially from that described in the preceding section for cluster **2** (Scheme 1). However, the higher reactivity of cluster **3** towards the

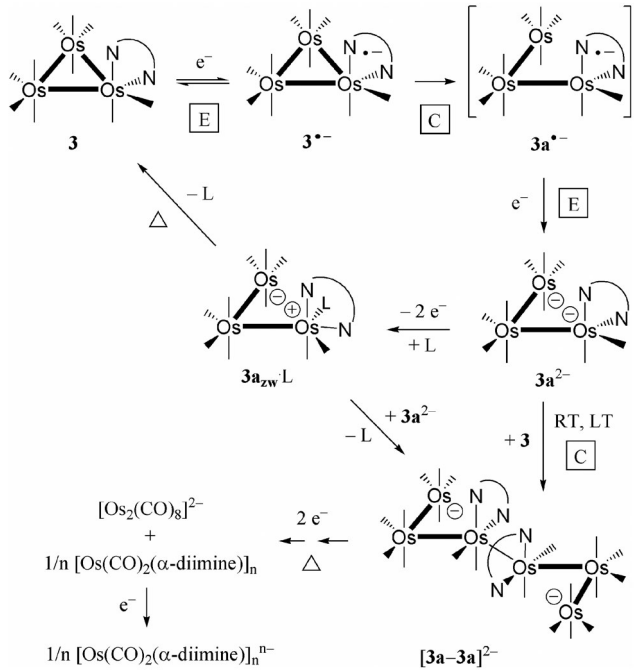

SCHEME 2
Electrochemical reduction and reoxidation paths of $[Os_3(CO)_{10}(bpy)]$ (**3**) constructed on the basis of the available experimental data, see below. The symbols E and C denote the (one-electron) electrochemical and chemical steps, respectively, in the reaction mechanism. The symbol Δ stands for a thermal reaction

cleavage of the Os–Os(α-diimine) bond makes it possible to investigate the initial steps (the ECE sequence) in more detail by cyclic voltammetry.

The cyclic voltammogram of **3** in THF shows an irreversible cathodic wave R_1 (Fig. 9). The apparent number of electrons transferred during this reduction process at room temperature was found to decrease with decreasing scan rate: n_{app} = 1.59 for v = 0.1 mV s^{-1} (Fig. 9a) and n_{app} = 1.21 for v = 50 V s^{-1}. The employed procedure (see Experimental) also yielded the diffusion coefficient for **3**, $D_3 = (0.22 \pm 0.04)/D_{Fc}$, which nicely corresponds with D_2, see above. The anodic counter-peak O_1 due to reverse oxidation of the primary one-electron reduction product $\mathbf{3}^{\bullet-}$ and the following cathodic wave R_2 due to its irreversible reduction to $\mathbf{3}^{2-}$ become observable at $v \geq$ 10 V s^{-1} (not shown), or at low temperatures (Fig. 9b, T = 205 K). (The assignment of the other anodic peaks on the reverse potential scan, viz. O_2* and O_3**, is discussed below.) These results mean that radical anion $\mathbf{3}^{\bullet-}$ undergoes a chemical reaction, probably cleavage of an Os–Os(bpy) bond, transforming to open-core $\mathbf{3a}^{\bullet-}$ directly reducible to corresponding dianion $\mathbf{3a}^{2-}$ (a two-electron ECE sequence, as proposed in Scheme 2). In this regard it is important to note that the reduction of the related cluster [$Os_3(CO)_{10}$-(*i*Pr-PyCa)] (Chart 1) containing a less basic α-diimine ligand (reducible at $E_{1/2}$ = –1.73 V vs –1.85 V for bpy in cluster **3**) is characterised under the

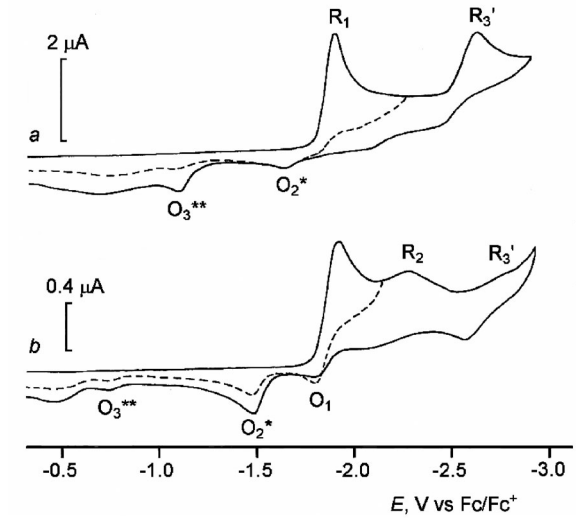

FIG. 9
Cyclic voltammograms of cluster **3**. Conditions: Pt disk electrode, THF, v = 100 mV s^{-1}, T = 293 K (a) and 205 K (b)

same experimental conditions by n_{app} = 1.92 (ref.[11]). The fact that a lower n_{app} value (1.59) has been determined for cluster **3**, does not reflect higher stability of $\mathbf{3}^{\bullet-}$ but, contrariwise, higher reactivity of $\mathbf{3a}^{2-}$. The open-core dianion attacks at the cathode yet non-reduced cluster **3** and forms dimer $[\mathbf{3a}–\mathbf{3a}]^{2-}$, in line with the overall one-electron ECEC sequence presented in Scheme 1. This argumentation has received strong support from the chemical reduction of cluster **3** with $[Fe(\eta^5\text{-}C_5H_5)(\eta^6\text{-}C_6Me_6)]$. Importantly, full conversion of cluster **3** in THF was achieved at 293 K with exactly one molar equivalent of the one-electron reducing agent. The ν(CO) region of the IR spectrum of the EPR-silent product, $[\mathbf{3a}–\mathbf{3a}]^{2-}$, indeed closely resembles that of $[\mathbf{2a}–\mathbf{2a}]^{2-}$ (Table II), the slightly smaller wavenumbers of the former cluster dimer reflecting the higher bpy donor ability compared with the bpym ligand. The result of the chemical reduction also excludes formation of a protonised open-core cluster, e.g., anion $H\mathbf{3a}^-$, as this product would require consumption of two molar equivalents of the reducing agent.

The electrochemical reduction of cluster **3** at room temperature was again monitored by IR and UV-VIS spectroscopy. Differently from cluster **2**, only a single product was formed both in THF and PrCN, independently of slow potential-sweep or rapid potential-step electrolysis. The ν(CO) wavenumbers of the product are nearly identical with those of $[\mathbf{3a}–\mathbf{3a}]^{2-}$ obtained by chemical reduction (Table II). The assignment is also confirmed by the UV-VIS spectrum of $[\mathbf{3a}–\mathbf{3a}]^{2-}$ (Fig. 10), which closely resembles that of $[\mathbf{2a}–\mathbf{2a}]^{2-}$ (cf. Fig. 8). The absorption band at 290 nm due to the ππ*(bpy)

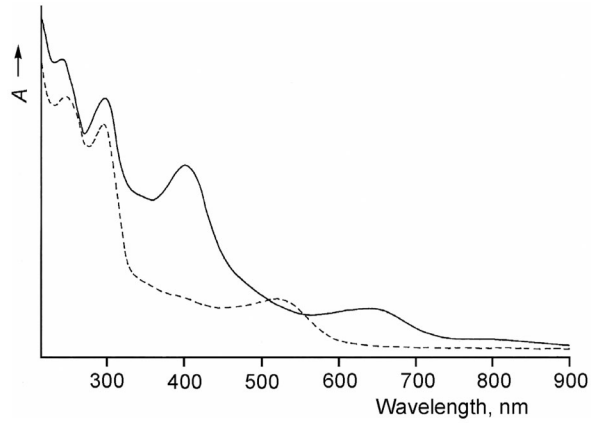

FIG. 10
UV-VIS spectra of parent cluster **3** (dashed line) and dimer $[\mathbf{3a}–\mathbf{3a}]^{2-}$ (full line) recorded in THF at T = 293 K within an OTTLE cell

transition was not affected by the reduction, which suggests that the bpy ligand in [**3a**–**3a**]$^{2-}$ remains non-reduced, in agreement with the molecular structure presented in Scheme 2. It is noteworthy that no **3**$^{\bullet-}$ (in THF) and **3a**$^{2-}$ (in PrCN) were detected in the IR spectra recorded in the course of the reduction at room temperature, in contrast to the observations made with cluster **2** (see above). This result agrees with the higher reactivity of both reduced species containing the stronger donor bpy ligand, as indicated by cyclic voltammetric data (Table I). Differently from the reduction-induced transformation of [**2a**–**2a**]$^{2-}$ to **P2a** (see Fig. 7), electrochemical reduction of [**3a**–**3a**]$^{2-}$ resulted directly in the fragmentation of the triosmium core, yielding $[Os_2(CO)_8]^{2-}$ and the reduced polymeric chain $[Os(CO)_2(bpy)]_n^{n-}$ (Scheme 2). The latter species[7] exhibits ν(CO) wavenumbers nearly identical to those of $[Os_2(CO)_8]^{2-}$ (1935 and 1854 cm^{-1}). Visually, the formation of the reduced polymer was also manifested by a blue layer deposited at the Pt cathode*.

Dimer [**3a**–**3a**]$^{2-}$ was also the exclusive product formed by reduction of cluster **3** in PrCN at 253 K. Lowering the temperature of the electrode compartment of the OTTLE cell to 200 K led to the observation of a mixture of [**3a**–**3a**]$^{2-}$ with another species of a similar IR ν(CO) pattern, but shifted to smaller wavenumbers. Its assignment to **3a**$^{2-}$ is supported by similar, only slightly larger ν(CO) wavenumbers of **2a**$^{2-}$ (Table II), and also by the important fact that reverse oxidation of **3a**$^{2-}$ gave dimer [**3a**–**3a**]$^{2-}$. These data clearly show that, differently from more stable **2a**$^{2-}$ (see above), dianion **3a**$^{2-}$ is still able to react with parent cluster **3** even at 200 K, even though much less efficiently than at room temperature where it was not observed at all. The zero-electron coupling reaction occurs not only during the reduction of cluster **3** but also during the reoxidation of **3a**$^{2-}$ following a reverse ECEC sequence similar to that operating along the reduction path in Scheme 2. We should remind that less reactive dianion **2a**$^{2-}$ transforms during the reoxidation in PrCN at 223 K exclusively to parent cluster **2**, the

* The formation of $[Os(CO)_2(bpy)]_n^{n-}$ triggers electrocatalytic reduction of carbon dioxide dissolved in the THF solution of **3**. IR spectroelectrochemical monitoring of the cathodic electrolysis revealed rapid disappearance of the CO_2 band at 2335 cm^{-1} and formation of Bu_4N^+ formate absorbing at 1607 and 1333 cm^{-1}, accompanied by Bu_4N^+ hydrogen- carbonate (1685 and 1646 cm^{-1}) and development of CO gas at the Pt minigrid. At more negative potentials, bands of $(Bu_4N^+)_2$ oxalate started to grow at 1550 and 1290 cm^{-1}. However, the latter species is most likely formed by direct reduction of CO_2 to the corresponding radical anion.

reaction barrier for the zero-electron coupling reaction being too high in this case.

Based on the spectroelectrochemical results, the cathodic wave R_3' in the cyclic voltammogram of cluster **3** (Fig. 9) probably belongs to the reduction of dimer [**3a**–**3a**]$^{2-}$, becoming diminished at low temperatures due to higher stability of dianion [**3a**–**3a**]$^{2-}$. The dimer is oxidised on the reverse scan at the anodic wave O_3**, in agreement with the thin-layer cyclic voltammogram of **3** in THF recorded at room temperature with v = 2 mV s^{-1} (Fig. 11). The more negative anodic peak O_2* then belongs to oxidation of dianion **3a**$^{2-}$, which is also supported by its increasing current intensity at low temperature. The shift of the irreversible anodic waves O_2* and O_3** to less negative potentials at reduced temperature (Fig. 9b) is not unusual.

Oxidation Path of Open-Core Cluster Dianions

The oxidation of dianion **3a**$^{2-}$ at the anodic wave O_2* was shown above to yield dimer [**3a**–**3a**]$^{2-}$ independently of the temperature used. The initial step in the mechanism must be the formation of one-electron-oxidised open-core radical anion **3a**$^{\bullet-}$, i.e., the reversal of the reduction path. The product can either directly dimerise to [**3a**–**3a**]$^{2-}$ or first oxidise to zwitterion $\mathbf{3a_{zw}}$, the latter compound reacting simultaneously with yet non-oxidised **3a**$^{2-}$ to give [**3a**–**3a**]$^{2-}$. To make this oxidation path thermodynamically feasible, it is important that **3a**$^{\bullet-}$ interacts with a Lewis base (e.g., the donor solvent) at the coordinatively unsaturated Os^{+}(CO)$_2$(bpy$^{\bullet-}$) site. The transient **3a**$^{\bullet-}$·L is then capable of undergoing one-electron oxidation to zwitterion $\mathbf{3a_{zw}}$·L already at the applied anodic potential of starting dianion **3a**$^{2-}$.

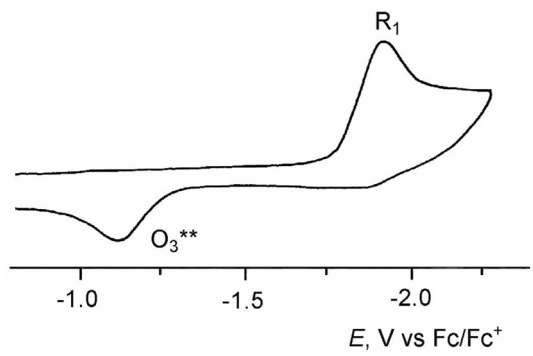

FIG. 11
Thin-layer cyclic voltammogram of cluster **3** recorded in an OTTLE cell. Conditions: THF , T = 293 K, v = 2 mV s^{-1}, Pt minigrid. The anodic wave O_3** belongs to dimer [**3a**–**3a**]$^{2-}$

Important evidence for this ECE oxidation path of open-core dianions (presented in a single two-electron step in Scheme 2) has been gained from the oxidation of $\mathbf{2a}^{2-}$ in PrCN at 223 K, yielding exclusively parent cluster **2**. Dimer $[\mathbf{2a}–\mathbf{2a}]^{2-}$ was obtained only at room temperature (see above). This difference from $\mathbf{3a}^{2-}$ is understandable, as bpym is a stronger π-acceptor than bpy and facilitates coordination of L at Os^{+} both in $\mathbf{2a}^{\bullet-}$ and $\mathbf{2a_{zw}}$. This interaction prevents the direct dimerisation of $\mathbf{2a}^{\bullet-}$ and also hinders the zero-electron reaction of $\mathbf{2a_{zw}}$·L with $\mathbf{2a}^{2-}$ in the course of the anodic process. Zwitterion $\mathbf{2a_{zw}}$·L (L = PrCN or THF) then undergoes thermal charge recombination resulting in the recovery of parent cluster **2**. Photochemically generated zwitterions $\mathbf{2a_{zw}}$·MeCN live ca. 20 s at 293 K [12d] but the lifetime may be significantly reduced along the anodic path.

We attempted to prove the transient formation of zwitterions upon oxidation of $\mathbf{3a}^{2-}$ by cyclic voltammetry. Figure 12a shows the cyclic voltammogram of cluster **3** at 293 K in THF saturated with CO. Comparison with Fig. 9a reveals that the reverse anodic scan, which started beyond the cathodic wave R_1, results in a significantly more intense anodic wave O_2* due to the oxidation of $\mathbf{3a}^{2-}$, and in a diminished anodic wave O_3** due to the oxidation of $[\mathbf{3a}–\mathbf{3a}]^{2-}$. In the light of the above discussion, this difference can

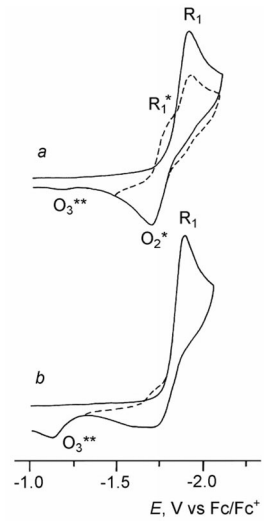

FIG. 12
Cyclic voltammogram of cluster **3** recorded in CO-saturated THF (a) and after purging with N_2 (b). Conditions: T = 293 K, v = 100 mV s^{-1}, Pt minigrid. The cathodic wave R_1* probably belongs to zwitterion $\mathbf{3a_{zw}}$·CO

be ascribed to stronger coordination of CO to zwitterion $\mathbf{3a_{zw}}$ compared with THF, which prevents its concomitant reaction with yet non-oxidised $\mathbf{3a}^{2-}$. Zwitterion $\mathbf{3a_{zw}}$·CO is then reduced during the repeated cathodic scan at the cathodic wave R_1*, which is shifted less negatively than R_1 of parent cluster **3**. This shift agrees with reduction of the positively charged $Os^+(CO)_3(bpy)$ site in $\mathbf{3a_{zw}}$·CO. Addition of strongly coordinating pyridine into the THF solution of **3** has a similar effect. As expected, zwitterion $\mathbf{3a_{zw}}$·pyridine reduces more negatively than $\mathbf{3a_{zw}}$·CO (see Table I). When the CO-saturated THF solution of **3** in the voltammetric cell is purged with nitrogen, the stabilisation of zwitterion $\mathbf{3a_{zw}}$ is cancelled. As documented in Fig. 12b, the removal of CO resulted in the growing anodic wave O_3** due to the oxidation of $[\mathbf{3a}–\mathbf{3a}]^{2-}$, while the anodic wave of $\mathbf{3a}^{2-}$ and the cathodic response of zwitterion $\mathbf{3a_{zw}}$·CO largely disappeared. All these changes fully agree with the proposed oxidation path of dianions $\mathbf{2a}^{2-}$ and $\mathbf{3a}^{2-}$.

Electrochemical and Photochemical Os–Os(α-diimine) Bond Cleavage in $[Os_3(CO)_{10}$(α-diimine)]

The presence of α-diimine ligands in transition metal carbonyl complexes is one of the key factors that determine spectroscopic, photochemical and electrochemical properties of this class of compounds. The major influence of the variation of α-diimine on the reactivity of electrochemically reduced and photoexcited complexes has been proven by a series of comprehensive experimental and theoretical investigations of a wide range of mononuclear compounds with d^6-metal centres, or metal–metal bonded d^7-species such as $[(CO)_5Mn–M(CO)_3(\alpha\text{-diimine})]$ (M = Mn, Re) or $[(CO)_5Mn–RuR(CO)_2(\alpha\text{-diimine})]$ (R = alkyl)[33]. The alkyl group and/or carbonyl metal fragment as strong σ-donor ligands X introduce strong X–M (M = Mn, Re) or $X_1–Ru–X_2$ axial σ-bonds (i.e., perpendicular to the M(α-diimine) plane), the corresponding delocalised σ-bonding molecular orbitals lying higher than the metal d_π-orbitals. The lowest excited state of the complex then has a sigma-bond-to-ligand charge-transfer (SBXCT) or σπ* character, where π* is largely the lowest unoccupied molecular orbital (the LUMO) of the α-diimine ligand. Upon light excitation, occupation of the σπ* excited state weakens the axial M–X bond and often results in its homolysis yielding radical fragments. In addition to the depopulation of the bonding σ-orbital, the weakening of the M–X bond in the σπ* state is also caused by a hyperconjugative $\pi^*(\alpha\text{-diimine}^{\bullet-})\sigma^*(M–X)$ interaction causing a partial delocalisation of the $\pi^*(\alpha\text{-diimine}^{\bullet-})$ electron density to the antibonding

σ*(M–X) orbital. The hyperconjugative interaction is more efficient with increasing energy of the π*(α-diimine$^{\bullet-}$) level. The relative importance of the σπ* and π*σ* effects cannot be assessed easily. Although, in the case of highly photolabile complexes [ReR(CO)$_3$(α-diimine)], the stability of their radical anions, with the odd electron mainly in the π*(α-diimine$^{\bullet-}$) orbital, indicates that the σπ* effect is more important. On the contrary, the hyperconjugative π*(α-diimine$^{\bullet-}$)σ*(M–X) interaction plays obviously the key role in the reactivity of the electrochemically one-electron-reduced complexes.

The general knowledge obtained from the studies of the above complexes can be extended to more intricate transition metal clusters. Specifically for the investigated [Os$_3$(CO)$_{10}$(α-diimine)] (α-diimine = bpy, *i*Pr-PyCa (ref.[11]), bpym) series, their highest occupied molecular orbital (HOMO) has been shown by DFT calculations to be largely localised on the σ-system of the triosmium core, while the lowest unoccupied molecular orbital (LUMO) has a dominant π*(α-diimine) character. An exception in this cluster family is the non-aromatic ligands 1,4-di-R-1,4-diazabutadiene (R-dab) with π-bonding strongly delocalised over the Os(R-dab) metallacycle[34]. The photochemical reactivity pattern of the clusters [Os$_3$(CO)$_{10}$(R-dab)] is characterised by the initial formation of reactive biradicals [Os$^{\bullet}$(CO)$_4$–Os(CO)$_4$–Os(CO)$_2$-(R-dab)$^{\bullet}$] having one of the Os–R-dab bonds cleaved[35]. For the above listed aromatic α-diimine ligands, the primary photoproducts are open-core biradicals of the type [Os$^{\bullet}$(CO)$_4$–Os(CO)$_4$–Os^{+}(CO)$_2$(α-diimine$^{\bullet-}$)], originating from optically populated low-lying σ(core)-to-π*(α-diimine) charge-transfer excited states. These biradicals may bind a Lewis base (L) at the Os^{+}(CO)$_2$(α-diimine$^{\bullet-}$) site and convert, by intramolecular electron transfer, to longer-lived zwitterions [Os^{-}(CO)$_4$–Os(CO)$_4$–Os^{+}(L)(CO)$_2$(α-diimine)] (ref.[12]). Direct heterolytic cleavage of the Os–α-diimine bond upon light excitation is also possible[12e,36]. For the non-aromatic R-dab ligands, zwitterions are less common and require a strong Lewis base (e.g., pyridine) for stabilisation[12b]. Time-dependent density functional theory (TD-DFT) calculations performed on the weakly π-delocalised Os-bpy system in cluster **3** reveal population of the lowest σπ* excited state that causes weakening and concomitant splitting of the Os–bpy bond adjacent to the Os(bpy) plane[34].

Based on the experimental spectroscopic evidence described in the preceding sections, and in agreement with the DFT data, the electrochemical reduction of the studied clusters **1**–**3** and [Os$_3$(CO)$_{10}$(*i*Pr-PyCa)] (ref.[11]) is largely localised on the aromatic α-diimine ligand. The single occupation of the π*(α-diimine$^{\bullet-}$) orbital in the primary radical anions causes weakening of the same Os–Os(α-diimine) bond involved in the photochemical activa-

tion. The underlying hyperconjugative π*(α-diimine$^{\bullet-}$)σ*(Os–Os) interaction causes partial delocalisation of the π*(α-diimine$^{\bullet-}$) electron density into the antibonding σ*(Os–Os) orbital, the degree of which is mainly controlled by the π-acceptor ability of the α-diimine in the parent neutral clusters. Obviously, bpy and *i*Pr-PyCa are much less amenable to accommodate the extra electron in their high-energy π* LUMO than the other investigated ligands, bpym and, in particular, μ-bpym, as reflected in the rather negative reduction potentials of the former two clusters (Table I). The Os–Os(α-diimine) bond cleavage in the primary radical anions occurs simultaneously with second reduction converting the open-core transients **2a**$^{\bullet-}$ and **3a**$^{\bullet-}$ to corresponding dianions **2a**$^{2-}$ and **3a**$^{2-}$ (Schemes 1 and 2). The latter products can be stabilised at low temperatures. At ambient temperature, cluster dimers [**2a**–**2a**]$^{2-}$ and [**3a**–**3a**]$^{2-}$ are formed readily by a nucleophilic attack of the {Os(CO)$_2$(α-diimine)}$^{-}$ moiety in the open-core dianions at the neutral Os(α-diimine) site in the parent clusters. However, it is assumed that direct dimerisation of **2a**$^{\bullet-}$ and **3a**$^{\bullet-}$ takes place in solution when the parent clusters are reduced chemically with one molar equivalent of [Fe(η^5-C$_5$H$_5$)(η^6-C$_6$Me$_6$)] or other suitable reducing agents.

Apparently, the studied triosmium α-diimine clusters with the Os(CO)$_2$-(α-diimine) moiety and one axial Os–Os(CO)$_2$(α-diimine) bond have much in common with the class of carbonyl complexes with α-diimine ligands, where the σπ*/π*σ* hyperconjugation mechanisms govern the redox and photochemical activation[26,37]. Very similar reduction paths operate, for example, in the case of tricarbonyl Mn(I) and dicarbonyl Ru(II) α-diimine complexes[21b,38]. The same dependence on the α-diimine ligand was also found for the metal–metal bond cleavage in the radical anions of di- and trinuclear complexes [(CO)$_5$Mn–Re(CO)$_3$(α-diimine)] (α-diimine = bpy, bpym) and [(CO)$_5$Mn–ReBr(CO)$_3$(μ-bpym)Re(CO)$_3$] (ref.[24b]). Again, the most stable radical anion was generated by one-electron reduction of the trinuclear complex with μ-bpym. On the other hand, the radical anion [(CO)$_5$Mn–Re(CO)$_3$(bpy$^{\bullet-}$)] decomposed instantaneously into [Mn(CO)$_5$]$^{-}$ and the reactive radicals [Re(CO)$_3$(bpy)]$^{\bullet}$. Such fragmentation triggered by one-electron reduction is largely prevented by the triosmium cluster backbone. The open-core secondary reduction products [**2a**–**2a**]$^{2-}$ and [**3a**–**3a**]$^{2-}$ are formally also one-electron-reduced species (Schemes 1 and 2). In contrast to **2**$^{\bullet-}$ and **3**$^{\bullet-}$, and the open-core transients **2a**$^{\bullet-}$ and **3a**$^{\bullet-}$, the negative charge in the dimers probably resides on the remote Os(CO)$_4$ centre and not any longer on the α-diimine. As revealed by IR spectra, the bonding situation in these compounds is analogous to that in the photochemically

generated zwitterions $[Os^{-}(CO)_4–Os(CO)_4–Os^{+}(L)(CO)_2(\alpha\text{-diimine})]$ and, in particular, the anionic photoproduct $[Os^{-}(CO)_4–Os(CO)_4–OsBr(CO)_2(bpym)]^{-}$.

Conclusions

The presented results of the electrochemical and spectroelectrochemical investigations are important for the general understanding of the cathodic transformation of the clusters $[Os_3(CO)_{10}(\alpha\text{-diimine})]$ into the open-core reduced species and, upon further reduction, into linear polymers consisting of (α-diimine)Os–Os(α-diimine) units. The temperature- and solvent-dependent steps along the reduction path can be effectively controlled by varying the π-acceptor ability of the parent α-diimine ligand. The intimate mechanism of the Os–Os(α-diimine) bond cleavage in the primary radical anionic species involves labilising delocalisation of the electron density from the singly occupied $\pi^*(\alpha\text{-diimine}^{\bullet-})$ orbital to the axial σ*(Os–Os) orbital. Similar open-core cluster compounds as formed along the reduction path can also be obtained photochemically from a low-lying σ(Os–Os)-to-$\pi^*(\alpha\text{-diimine})$ charge transfer excited state, emphasizing the key role of the non-innocent α-diimine ligand. In this case, the depopulation of the bonding σ(Os–Os) orbital in the excited state is expected to operate together with the hyperconjugative $\pi^*(\alpha\text{-diimine}^{\bullet-})/\sigma^*(Os–Os)$ interaction. It is difficult to assess the relative importance of these effects for the photochemical cleavage of the Os–Os(α-diimine) bond.

Financial support for this work was obtained from the Council for Chemical Sciences of the Netherlands Organisation for Scientific Research (CW-NWO, grant JC 348-032) and from the European Union (COST working groups D14/0001/99 and D29/0012/04).

REFERENCES

1. a) Venäläinen T., Pakkanen T. A., Pakkanen T. T., Iiskola E.: *J. Organomet. Chem.* **1986**, *314*, C49; b) Kiiski U., Venäläinen T., Pakkanen T. A., Krause O.: *J. Mol. Catal.* **1991**, *64*, 163; c) Alvila L., Pakkanen T. A., Krause O.: *J. Mol. Catal.* **1993**, *84*, 145; d) Alvila L., Pursiainen J., Kiviaho J., Pakkanen T. A., Krause O.: *J. Mol. Catal.* **1994**, *91*, 335; e) Haukka M., Alvila L., Pakkanen T. A.: *J. Mol. Catal. A* **1995**, *102*, 79.
2. Haukka M., Venäläinen T., Hirva P., Pakkanen T. A.: *J. Organomet. Chem.* **1996**, *509*, 163.
3. a) Luukkanen S., Homanen P., Haukka M., Pakkanen T. A., Deronzier A., Chardon-Noblat S., Zsoldos D., Ziessel R.: *Appl. Catal., A* **1999**, *185*, 157; b) Chardon-Noblat S., Da Costa P., Deronzier A., Haukka M., Pakkanen T. A., Ziessel R.: *J. Electroanal. Chem.* **2000**, *490*, 62.
4. Masciocchi N., Sironi A., Chardon-Noblat S., Deronzier A.: *Organometallics* **2002**, *21*, 4009.

5. Chardon-Noblat S., Deronzier A., Ziessel R.: *Collect. Czech. Chem. Commun.* **2001**, *66*, 207; and references therein.
6. Chardon-Noblat S., Da Costa P., Deronzier A., Mahabiersing T., Hartl F.: *Eur. J. Inorg. Chem.* **2002**, 2850.
7. Hartl F., Mahabiersing T., Chardon-Noblat S., Da Costa P., Deronzier A.: *Inorg. Chem.* **2004**, *43*, 7250.
8. Bruce M. I., Humphrey M. G., Snow M. R., Tiekink E. R., Wallis R. C.: *J. Organomet. Chem.* **1986**, *314*, 311.
9. Vergeer F. W., Calhorda M. J., Matousek P., Towrie M., Hartl F.: *Dalton Trans.* **2003**, 4084.
10. van Outersterp J. W. M.: *Ph.D. Thesis*. University of Amsterdam, Amsterdam 1995.
11. Nijhoff J., Hartl F., van Outersterp J. W. M., Stufkens D. J., Calhorda M. J., Veiros L. F.: *J. Organomet. Chem.* **1999**, *573*, 121.
12. a) Bakker M. J., Hartl F., Stufkens D. J., Jina O. S., Sun X.-Z., George M. W.: *Organometallics* **2000**, *19*, 4310; b) Nijhoff J., Bakker M. J., Hartl F., Stufkens D. J., Fu W.-F., van Eldik R.: *Inorg. Chem.* **1998**, *37*, 661; c) Nijhoff J., Hartl F., van Outersterp J. W. M., Stufkens D. J., Calhorda M. J., Veiros L. F.: *J. Organomet. Chem.* **1999**, *573*, 121; d) van Outersterp J. W. M., Garriga Oostenbrink M. T., Nieuwenhuis H. A., Stufkens D. J., Hartl F.: *Inorg. Chem.* **1995**, *34*, 6312; e) Vergeer F. W., Kleverlaan C. J., Matousek P., Towrie M., Stufkens D. J., Hartl F.: *Inorg. Chem.* **2005**, *44*, 1319.
13. Astruc D., Hamon M., Lacoste M., Desbois M.-H., Román E. in: *Organometallic Synthesis* (R. B. King, Ed.), p. 172. Elsevier, Amsterdam 1988.
14. Bossard C., Rigaut S., Astruc D., Delville M.-H., Félix G., Février-Bouvier A., Amiell J., Flandrois S., Delhaès P.: *J. Chem. Soc., Chem. Commun.* **1993**, 333.
15. Leadbeater N. E., Lewis J., Raithby P. R., Ward G. N.: *J. Chem. Soc., Dalton Trans.* **1999**, 2511.
16. Treichel P. M., Williams J. P.: *J. Organomet. Chem.* **1977**, *135*, 39.
17. a) *Public EPR Software Tools*. National Institute of Environmental Health Sciences, available at http://epr.niehs.nih.gov/pest.html (access date September 2002); b) Duling D. R.: *J. Magn. Reson., Ser. B* **1994**, *104*, 105.
18. Krzystek J., Sienkiewicz A., Pardi L., Brunel L. C.: *J. Magn. Reson.* **1997**, *125*, 207.
19. Gritzner G., Kůta J.: *Pure Appl. Chem.* **1984**, *56*, 461.
20. Pavlishchuk V. V., Addison A. W.: *Inorg. Chim. Acta* **2000**, *298*, 97.
21. a) Amatore C., Azzabi M., Calas P., Jutand A., Lefrou C., Rollin I.: *J. Electroanal. Chem.* **1990**, *288*, 45; b) Rossenaar B. D., Hartl F., Stufkens D. J., Amatore C., Maisonhaute E., Verpeaux J.-N.: *Organometallics* **1997**, *16*, 4675.
22. Krejčík M., Daněk M., Hartl F.: *J. Electroanal. Chem. Interfacial Electrochem.* **1991**, *317*, 179.
23. a) Hartl F., Luyten H., Nieuwenhuis H. A., Schoemaker G. C.: *Appl. Spectrosc.* **1994**, *48*, 1522; b) Mahabiersing T., Luyten H., Nieuwendam R. C., Hartl F.: *Collect. Czech. Chem. Commun.* **2003**, *68*, 1687.
24. a) van Outersterp J. W. M., Hartl F., Stufkens D. J.: *Inorg. Chem.* **1994**, *33*, 2711; b) van Outersterp J. W. M., Hartl F., Stufkens D. J.: *Organometallics* **1995**, *14*, 3303.
25. Kaim W., Kohlmann S., Lees A. J., Snoeck T. L., Stufkens D. J., Zulu M. M.: *Inorg. Chim. Acta* **1993**, *210*, 159.
26. Klein A., Vogler C., Kaim W.: *Organometallics* **1996**, *15*, 236.
27. Kohlmann S., Kaim W.: *Inorg. Chem.* **1990**, *29*, 2909.

28. Bhattacharyya N. K., Coffy T. J., Quintana W., Salupo T. A., Bricker J. C., Shay T. B., Payne M., Shore S. G.: *Organometallics* **1990**, *9*, 2368.
29. Greef R., Peat R., Peter L. M., Pletcher D., Robinson J. in: *Instrumental Methods in Electrochemistry* (T. J. Kemp, Ed.), Chap. 6., p. 180. Ellis Horwood Ltd., Chichester 1985.
30. Braterman P. S., Song S.-I., Kohlmann S., Vogler C., Kaim W.: *J. Organomet. Chem.* **1991**, *411*, 207.
31. Vergeer F. W., Lutz M., Spek A. L., Calhorda M. J., Stufkens D. J., Hartl F.: *Eur. J. Inorg. Chem.* **2005**, 2206.
32. Amatore C., Krusic P. J., Pedersen S. U., Verpeaux J.-N.: *Organometallics* **1995**, *14*, 640.
33. Vlček A., Jr.: *Coord. Chem. Rev.* **2002**, *208*, 309; and references therein.
34. a) Calhorda M. J., Hunstock E., Veiros L. F., Hartl F.: *Eur. J. Inorg. Chem.* **2001**, 223; b) Bakker M. J., Calhorda M. J., Hartl F.: Unpublished results.
35. Nijhoff J., Bakker M. A., Hartl F., Stufkens D. J.: *J. Organomet. Chem.* **1999**, *572*, 271.
36. Nijhoff J., Hartl F., Stufkens D. J., Piet J. J., Warman J. M.: *Chem. Commun.* **1999**, 991.
37. a) Vlček A., Jr., Baumann F., Kaim W., Grevels F.-W., Hartl F.: *J. Chem. Soc., Dalton Trans.* **1998**, 215; b) Kaim W., Kohlmann S.: *Chem. Phys. Lett.* **1987**, *139*, 365; c) Kaim W., Kohlmann S.: *Inorg. Chem.* **1990**, *29*, 2909; d) Kaim W., Olbrich-Deussner B., Gross R., Ernst S., Kohlmann S., Bessenbacher C. in: *Importance of Paramagnetic Organometallic Radical Species in Activation, Selectivity and Catalysis* (M. Chanon, Ed.), p. 283. Reidel, Dordrecht 1989.
38. Aarnts M. P., Hartl F., Peelen K., Stufkens D. J., Amatore C., Verpeaux J.-N.: *Organometallics* **1997**, *16*, 4686.